The role of microbial activity in the generation of Lower Cretaceous mixed Fe-oxide–phosphate ooids from the Provençal Domain, French Maritime Alps

THE ROLE OF MICROBIAL ACTIVITY IN THE GENERATION OF LOWER CRETACEOUS MIXED FE-OXIDE – PHOSPHATE OOIDS FROM THE PROVENÇAL DOMAIN, FRENCH MARITIME ALPS

LUCA BARALE, ANNA D'ATRI & LUCA MARTIRE

Dipartimento di Scienze della Terra

Università degli Studi di Torino,

Via Valperga Caluso 35, 10125 Torino, Italy

Corresponding author: Luca Barale, luca.barale@unito.it

Key words: Mixed Fe-oxide – phosphate ooids, condensed deposits, bacterial activity, Lower Cretaceous, Provençal Domain.

ABSTRACT

Early Hauterivian mixed Fe-oxide – phosphate ooids from the Lower Cretaceous condensed succession of the Alpine Provençal Domain are ellipsoidal, 200-2000 μm in diameter, and the main component of a sedimentary body, 0-100 cm thick, that can be traced laterally for tens of kilometers. Cathodoluminescence, EDS microprobe, backscattered electron imaging, epifluorescence, XRD, and micro Raman spectroscopy reveal that ooid cortices consist of variable proportions of Fe-oxide-rich and Ca-phosphate-rich layers. SEM observations show that phosphate-rich layers are composed of a dense matrix of micrometer-size, rod-shaped,

commonly curved phosphate grains, whose size and shape strongly suggest a microbial origin. Conversely, Fe-oxide-rich ooid cortical layers consist of aggregates of micrometer-size, plate-like crystals of hematite that point to an inorganic precipitation. We suggest that the ooidal condensed interval records a long sedimentary history in an open shelf environment subject to a background accumulation of organic-rich, fine-grained sediments. It was periodically interrupted by high-energy, storm-related events that resulted in winnowing, reworking, and oxygenation that favored precipitation of Fe-oxides around nuclei of biogenic origin. Such precipitation was not uniform on the outer surface of ooids and influenced their ellipsoidal shape. After the return to background conditions, Fe-ooids were buried and driven from an oxic to a post-oxic subbottom geochemical environment where rod-shaped Fe-reducing bacteria colonized Fe-ooid outer surfaces. Decomposition of organic matter and release of P bound on Fe-oxides increased pore-water concentration of phosphate, which precipitated at the outer surfaces of the ooids, thus preserving the microbial community. The bimineralic composition of these ooids discloses a complex and prolonged history of cyclic alternations of oxic and post-oxic geochemical conditions, which are in turn related to alternating sediment accumulation and winnowing phases with exposure at the seafloor.

INTRODUCTION

Iron ooids are a relatively rare component of sedimentary rocks; they usually occur as the main constituents of thin stratigraphic intervals (ooidal ironstones) with wide chronologic (Precambrian to Cenozoic) and geographic (America, Europe, Asia, Africa, Australia) distribution (Van Houten and Bhattacharyya 1982; Dahanayake and Krumbein 1986; Van Houten 1990). Classic examples are the Toarcian-Aalenian “Minette ooidal ironstones”

(Bubenicek 1971) and the Bajocian ”Oolithe ferrugineuse de Bayeux” (Fürsich 1971) in the Jurassic successions of the Paris Basin.

Iron ooids are usually ellipsoidal, with major axis between 0.2 and 2 mm in length. They contain a nucleus of different types of particles, surrounded by a cortex consisting of a series of concentric layers whose thickness vary from few micrometers to a few tens of micrometers (Burkhalter 1995; Sturesson et al. 2000). Chemical composition is variable, with Fe-rich layers commonly alternating with P_2O_5-rich layers; when the latter prevail, the name “phosphatic ooids” is used (Horton et al. 1980; Karakus et al. 2001). Some layers may also be formed by clay or carbonate minerals. Fe-rich layers may be limonitic or be composed of berthierine and chamosite (Teyssen 1984; Burkhalter 1995; Sturesson et al. 2000; Karakus et al. 2001). Phosphatic layers are usually formed by francolite, a carbonate- and fluorine-rich apatite (Horton et al. 1980; Karakus et al. 2001). Phosphatic layers are commonly characterized by a fine dispersion of goethite or other Fe-minerals, which give them a dark color and make them difficult to distinguish from Fe-rich layers both macroscopically and in thin section. In this case, an effective method for recognizing of phosphatic layers is cathodoluminescence (CL) imaging (Karakus et al. 2001).

Most authors (e.g., Dahanayake and Krumbein 1986; Sturesson et al. 1999; Einsele 2000) share the view that ooids are formed within fine-grained sediments, in shallow-water environments characterized by repeatedly changing hydrodynamic energy levels. Episodic high-energy events would be responsible for winnowing and ooid concentration to give rise to grainstones, commonly as bedforms internally showing cross-lamination (Teyssen 1984; Donaldson et al. 1999). Environmental conditions should be mainly oxidizing, although the presence of ferrous-iron-bearing chamosite suggests development under partially reducing conditions.

Whereas the probable biogenic origin of Fe-rich cortical layers is generally accepted, and in some cases supported by direct observation of microorganism remains (Dahanayake and

Krumbein 1986; Préat et al. 2000), the genesis of the phosphatic layers has been considered either primary and probably biologically induced (e.g., Burkhalter 1995), or related to secondary diagenetic processes (Sturesson and Bauert 1994; Sturesson et al. 2000).

The general role of microbial activity (bacteria, fungi, cyanobacteria) in phosphogenesis is rather universally recognized (e.g., Lucas and Prévôt 1991; Föllmi 1996; Soudry 2000). The preservation, in phosphatic deposits, of fossils of various microorganisms that may contribute to the precipitation of phosphate has long been known (Cayeux 1936) and has been documented in deposits of many ages (Lucas and Prévôt 1991; Soudry 2000).

A first important contribution of microorganisms in phosphogenesis is the mobilization and concentration of phosphorus through decomposition of organic matter. In addition, passive, biological processes also seem to play an active role in the precipitation of phosphate minerals (Soudry 2000). Several experiments (Lucas and Prévôt 1985, 1991) pointed out the ability of certain bacteria to cause the precipitation of calcium phosphate by the release of enzymes (*in vivo* or *postmortem*). Branching tubular forms, a few micrometers in diameter, or coccoid forms arranged in globular colonies 15-20 µm in diameter were observed in pseudo-oolitic phosphate grains in phosphoritic deposits and were interpreted as being fossil microorganism remains (Soudry and Champetier 1983; Dahanayake and Krumbein 1985). Krajewski et al. (1994), however, suggest that similar structures may have an inorganic origin. Although structures attributed to microorganisms are commonly reported from phosphatic deposits, except for a few present-day cases (e.g., Namibian shelf; Schulz and Schulz 2005), no detailed understanding of their role has as yet been attained.

The goal of this paper is two-fold: 1) to report well-preserved microbial remains in the phosphatic layers of mixed Fe-oxide – phosphate ooids and to propose a hypothesis about their nature and metabolic pathways of the preserved microorganisms; 2) to discuss implications concerning the paleoenvironmental-sedimentological interpretation of oolitic ironstones. The results suggest that the ooids result from cyclic alternations of sediment accumulation, with

shallow burial of ooids, and winnowing, with exposure at the seafloor, in turn affecting biogeochemical processes in oxic and post-oxic conditions responsible for composition and shape of these mixed-mineralogy ooid cortexes.

GEOLOGICAL SETTING

The studied material comes from Lower Cretaceous condensed successions cropping out in SE France, near Nice (Département des Alpes-Maritimes, Fig. 1A). During the Mesozoic, this area, which corresponds to the southeastern margin of the Alpine External Domain (Dauphinois and Provençal Domains), was part of the European passive margin of the Alpine Tethys. Above a crystalline basement, thick continental successions of Upper Carboniferous-Permian age were deposited, followed by Lower Triassic clastic sediments, Middle Triassic carbonates, and Upper Triassic evaporites (Fig. 2). Starting in the Early Jurassic, as a result of extensional tectonics related to the opening of the Alpine Tethys (Dardeau 1988), the European passive margin began to differentiate into a platform domain (Provençal) and a basinal domain (Dauphinois).

In the Provençal Domain, after a period of emersion which included most of the Early Jurassic, Middle-Late Jurassic sedimentation occurred in a carbonate platform environment. Starting in the Oxfordian, regression culminated in the Berriasian transition to peritidal conditions. Subsequently, Valanginian tectonism in the Nice Arc area resulted in drowning of the carbonate platform and transition to open marine shelfal conditions (Debelmas and Kerckhove 1980). The Hauterivian-lower Cenomanian *pro parte* (*p.p.*) succession is represented by condensed deposits characterized by discontinuity surfaces and an abundance of authigenic minerals such as glaucony and phosphate. After early Cenomanian drowning of the shelf, sedimentation continued with the deposition of hemipelagic and pelagic sediments (early Cenomanian *p.p.*-Campanian).

The Fe-rich ooids are concentrated in a stratigraphic interval, 0-100 cm thick, at the base of the Hauterivian-Barremian succession (Fig. 2). It overlies a commonly mineralized regional polygenic discontinuity surface, which corresponds to a considerable stratigraphic gap (Lanteaume 1968; Dardeau 1984) developed during drowning of the Jurassic-Berriasian carbonate platform and the abrupt transition to a condensed platform succession of progressively deeper environment. On the basis of the ammonite associations, Dardeau (1984) attributed iron oolite deposits of the Nice Arc to the early Hauterivian (*A. radiatus* Zone). The overlying deposits (glauconitic-phosphatic packstone to wackestone – cephalopod limestone) document a progressive rise of relative sea level.

These iron oolite deposits have been known for a long time (Perez 1847; de Riaz 1900) and were classically indicated in the literature as "*oolithes ferrugineuses*" (Thomel 1961; Lanteaume 1968; Pasquini et al. 2004), without reference to their phosphatic component. Most recently, Decarlis and Lualdi (2008) described these ooids as exclusively phosphatic, despite their considerable Fe_2O_3 content, attributing them to an outer-shelf environment and relating their genesis to the influence of upwelling currents.

MATERIAL AND METHODS

The raw material comes from two different sections (Roccaniera and Albaretta, Fig. 1B) located inland from Nice, close to the classic section of the Jurassic-Cretaceous Provençal succession of Saint Laurent de l'Escarène (Fig. 1B; Lanteaume 1968; Dardeau 1984). In particular, samples were collected from the Lower Cretaceous part of the succession that consists of Fe-ooid-rich limestones.

Petrographic studies of polished thin sections were carried out by plane-polarized-light and cross-polarized-light microscopy. Convergent transmitted light (CTL) was used in order to minimize the light absorption by Fe-oxides and better distinguish ooid internal structures.

Cathodoluminescence observations were carried out using CITL 8200 mk3 equipment (~ 17 kV, 400 μA). They have proven useful for distinguishing between Fe-oxide-rich layers and phosphate-rich layers, which have a similar color in transmitted light but a clearly distinct luminescence (see Karakus et al. 2001). Epifluorescence observations of polished thin sections were also made to highlight the presence of organic matter and hence the role of microbial activity in the precipitation of authigenic minerals. Observations were performed using a Nikon Eclipse E400 epifluorescence microscope, equipped with the UV-2A, B-2A, and G-2A filter combinations (excitation wavelength of 330-380 nm, 450-490 nm, and 510-560 nm, respectively).

SEM observations (with a Cambridge S-360 instrument) were made on gold-coated rock fragments (obtained by mechanical split) in order to investigate the microstructure of both Fe-oxide-rich and phosphate-rich layers. In addition, *in situ* chemical analyses were carried out to determine chemical compositions by means of an EDS microprobe Link System connected to a scanning electron microscope (Cambridge S-360). In order to better characterize the minerals composing the mixed Fe-oxide phosphate ooids and to detect the possible presence of organic matter, micro Raman spectroscopy and X-ray diffraction (XRD) analyses were carried out. Micro Raman spectroscopy was performed with a LabRAM-HR 800 (HORIBA - JOBIN-YVON) spectrometer using a HeNe laser (633 nm, 20 mW). XRD was performed with a Siemens D5000 X-ray diffractometer that is a theta/2theta diffraction instrument operating in reflection (Bragg-Brentano) geometry using Cu-Kα1.2 radiation. The Cu tube is run at 40 kV and 30 mA. The slit arrangement is 1 mm pre-sample slit, 0.6 mm post-sample slit, and a 0.6 mm detector slit. The detector is a standard scintillation counter.

OBSERVATIONS

The Fe ooidal deposits comprise a stratigraphic interval 0 to 1 m thick made up of bioturbated oolitic wackestones, laterally transitioning into bioturbated oolitic packstones. Ooids are the more abundant grains (Fig. 3), with only a small percentage of skeletal grains, intraclasts and Fe-oxyhydroxide clasts (intraclasts derived from the underlying mineralized discontinuity surface or mineralized skeletal grains). Fossils are common, including ammonites (*Lytoceras* sp., *Phylloceratidae*), nautiloids (*Cymatoceras* sp.), belemnites (such as *Duvalia* sp.), echinoderms, brachiopods, bivalves, and fish teeth. In particular, cephalopods are invariably reworked, as is demonstrated by the marked compositional, textural, and color contrast of the internal mold with the encasing sediment (Fig. 3). The matrix is carbonate in composition and consists of a micrite with sparse fragments of skeletal grains (bivalves, foraminifers, ammonoids) and silt-size peloids. These sediments are intensely bioturbated and do not preserve any other sedimentary structure. This interval is discontinuous but as a whole can be traced laterally for some tens of kilometers over the Nice Arc area of the Provençal Domain without significant lithologic and age changes (Thomel 1961).

The ooids are oblate ellipsoidal grains, with major axis ranging between 200 and 2000 µm in length, more commonly between 500 and 800 µm. Color is brown on the hand sample, and reddish brown to tan in thin section under convergent transmitted light (CTL). The internal structure is characterized by a nucleus surrounded by a series of concentric cortical layers, whose thickness ranges from some micrometers to a few tens of micrometers. Layers are locally discontinuous and irregular in thickness. In some instances, discrete sets of cortical layers cannot be followed all around the ooid but are developed on opposite sides (Fig. 4). Some encrusting foraminifera were also observed in the cortices. They appear as lenticular tests about 50-100 µm in width, replaced and filled with Fe-oxides and referable to *Nubecularia* sp. (Fig. 5). Ooid nuclei are in most cases Fe-oxyhydroxide clasts (Fig. 4A, B) and fragments of other ooids, and less common entire or fragmentary fish teeth (Figs. 6, 7A-D), or mineralized wackestone intraclasts. Fe-oxyhydroxide clasts are in places characterized by a “spongy” structure where

voids, a few tens of micrometers in diameter, are filled with phosphate. Fish teeth consist of a well preserved, primary phosphatic, enamel part and a dentine part, showing the characteristic tubular structure, impregnated and substituted by Fe-oxides (Figs. 6, 7C, D). In all observed mineralized teeth, the first ooid cortical layers are developed on the Fe-oxide-impregnated side (Figs. 6, 7C, D). In the grain-supported facies, in which the ooids are in contact with each other, a conspicuous fraction of ooids shows concavo-convex contacts with the surrounding ooids that mainly result from their plastic deformation (Fig. 4).

SEM-EDS microanalysis revealed two kinds of cortical layers of different composition, associated in different proportions in the ooids: Fe-rich layers, composed mainly of Fe-oxides (Fe_2O_3 between 60% and 75%, with smaller percentages of Al_2O_3 (2-5%), SiO_2 (2-8%), and P_2O_5 (1-3%)), and phosphatic layers, formed by Ca-phosphate with a variable amount of Fe-oxides (P_2O_5: 15-35%, Fe_2O_3: 1-45%). These compositionally different layers are clearly distinguished by backscattered electron imaging, the Fe-rich portions being brighter than phosphate-rich ones (Figs. 4B, 6, 7C, E).

To characterize the mineralogical composition of the ooidal sediments, X-ray diffractometry (XRD) and micro Raman spectroscopy (MRS) were carried out. XRD was performed on bulk rock samples consisting of mixed ooids and inter-ooidal matrix and cement, whereas MRS analyses were made on selected ooids already observed and analyzed with SEM-EDS and cathodoluminescence. XRD shows the presence of calcite, hematite, goethite, and a poorly crystalline phosphate phase that could not be better defined. MRS spectra show peaks of hematite and of a mineral of the apatite group that, because of the poor crystallinity, cannot be further specified. The comparison of the results of the two analytical techniques shows that goethite and calcite do not contribute to the ooid cortices but are present only as intergranular matrix and/or cement, and therefore ooid cortices consist substantially of hematite and poorly crystalline apatite in variable proportions. Moreover, two MRS bands occurring at around 1350

cm^{-1} and near 1600 cm^{-1} document also the presence of carbonaceous matter in the ooid phosphate-rich cortical layers (Fig. 8).

The comparison of backscattered electron images, integrated by EDS analyses, and of CL images of the same Fe-ooids highlights a strict correlation between nonluminescence and Fe-rich cortical layers whereas phosphate-rich cortical layers show a distinct moderate to dull bluish luminescence comparable to that of fish teeth (Fig. 7B, F, G, I) (see Karakus et al. 2001). Cathodoluminescence is thus very useful for a quick observation of thin sections aimed at an easy detection of the distribution of phosphate-rich and Fe-rich layers. These observations revealed that these deposits include ooids formed mainly of phosphate-rich layers, ooids formed mainly of Fe-rich layers, and ooids formed of both Fe-rich and phosphate-rich layers, each in roughly equal proportions (Fig. 7G, I).

Epifluorescence observations highlight the presence of luminescing and nonluminescing layers within ooid cortices. Again, the comparison with backscattered electron and EDS data indicates that phosphatic cortical layers and fish teeth are luminescent, whereas Fe-rich phases are not (Fig. 7D, H, J). Epifluorescence imaging, moreover, is even more precise than CL in highlighting the phosphate-rich layers.

SEM images demonstrate that hematite layers consist of crystals with a platy habit, 0.5 to 2 µm in diameter, aggregated into typical rosette-like structures (Fig. 9). Phosphatic layers instead show a characteristic “microcracked” surface (cf. Purnachandra Rao et al. 2000), with a network of “cracks” that divides it into portions of submicrometric size (Fig. 10D-I). SEM observations confirm the presence of alternating thin (tens of micrometers) Fe-rich and phosphate-rich cortical layers, evinced by cathodoluminescence, backscattered electron images, and epifluorescence, but show a more intimate association of Fe-oxides and phosphates (Fig. 10A, B). Hematite plates in Fe-rich layers appear to be coated by a microcracked film of phosphate. Moreover, phosphate-rich layers are composed of phosphate grains bound in a structureless phosphate matrix (Fig. 10C-I). These grains display a variety of shapes and sizes. The most common type of phosphate

grain are commonly curved and slightly compressed rods, 2-3 µm long and 0.5-0.8 µm in diameter, commonly displaying a longitudinal groove (Fig. 10C-H). In a few cases it is possible to observe broken rods that appear to be hollow. The rods can be either densely packed in continuous layers (Fig. 10C) or associated as clusters (Fig. 10D-F). In continuous layers, rods exhibit random orientations on surfaces and are flattened parallel to it. In cross section, however, some rods have their long axes oriented transversally to the surface. Clusters may result from random arrangement of rods, juxtaposition of rods along the long axis, or alignment of rods to form elongated chains of several grains (Fig. 10D-F). This type of grain, recognizable also under the optical microscope, was observed both in the phosphatic layers and in the phosphates filling the voids of "spongy" Fe-oxide grains as the nuclei of some ooids. Thin filaments (0.2-0.3 µm in diameter and 4-5 µm long; Fig. 10I), and bowl-shaped hemispheric hollow grains (1 to 1.5 µm in diameter, commonly associated in small clusters; Fig. 10I) are less common.

DISCUSSION

Several aspects of the origin of Fe-ooids and authigenic phosphates have not attained a general consensus yet such as the external shape and internal structure of Fe-ooids, the depositional and diagenetic conditions in which they form, and any microbial contribution in their genesis. One of the most striking differences between carbonate ooids and Fe-ooids, apart from composition, is the shape, which is markedly oblate in Fe-ooids. This study shows that this shape is primary, and not due to burial flattening, since it is equally found in ooids oriented with the equatorial plane parallel or nearly perpendicular to bedding and in beds, or portions of beds, that lack any independent evidence of compaction. Beds, or portions of beds, containing ooids with particularly flattened shapes are grain-supported and commonly display concave-convex contacts among ooids. This observation suggests that compaction indeed played a role, but just in enhancing the flattening of the primarily oblate ellipsoids. This plastic deformation of ooids

indicates that they were not completely rigid when mechanical compaction started and suggests that a progressive hardening took place during burial (cf. Baturin 1982). Microcracks displayed by the phosphate layers could document a progressive water loss from a precursor, gel-like, Ca-phosphate and concomitant hardening during diagenesis. As to the interpretation of the oblate ellipsoidal shape, previous authors (Sturesson et al. 2000) proposed a non-uniform growth around nuclei, with faster growth rates at the equatorial section. Several ooid features (Fig. 4) seem to be consistent with the hypothesis of an asymmetric growth, but further suggest that Fe-oxides precipitation took place only on the upper, exposed, parts of Fe-ooids half-buried in sediment. Reworking and overturning then caused the growth on opposite sides of the ooids, finally resulting in nonspherical shapes.

One interesting observation lies in exceptionally well-preserved nanostructures in the cortices of Fe-ooids. The microfabric of Fe-rich layers composed of platy hematite crystals indicates inorganic Fe-oxide precipitation. Conversely, size, shape, and arrangement of phosphate grains suggest a microbial origin. The most common phosphate grains, as straight or curved rods, closely resemble bacillus-like bacterial forms, more than any other structures formed by inorganic crystal growth (e.g., Krajewski et al. 1994; Purnachandra Rao et al. 2000; Soudry 2000). Moreover, the arrangement of these grains as dense continuous mats, clusters of a few grains surrounded by a structureless phosphate matrix, and elongated chains of several grains supports a biogenic origin. Filamentous and bowl-shaped forms, albeit less common in the studied samples, are other morphologies typical of microbial cells (Soudry 1992, 2000; Konhauser 2007). A confirmation of their microbial origin comes from the presence of organic matter in phosphate-rich cortical layers, suggested by the markedly brighter fluorescence and proven by micro Raman spectroscopy (Fig. 8). The latter shows bands occurring at around 1350 cm^{-1} and 1600 cm^{-1} characteristic of poorly crystalline carbonaceous material (cf. Beyssac et al. 2002, with references) together with a narrow peak at 964 cm^{-1} related to apatite.

In this Lower Cretaceous example, it is possible to hypothesize about the nature and metabolism of microorganisms preserved as phosphate as well as the relation between phosphate precipitation and the presence of Fe-oxides. Fe-oxide cortical layers locally grade laterally into phosphate (Fig. 7G). At a finer scale, individual Fe-oxide layers, only a few micrometers thick, exhibit irregular spongy structures with microcavities filled with rod-shaped phosphatic microbial remains. This texture contrasts with that of "massive" pure Fe-oxide layers (Fig. 11), suggesting a process of "corrosion" of Fe-oxide layers followed by cementation by phosphate.

A conceptual model of preferential growth of phosphate on Fe-oxide substrates is consistent with the observation that all observed fish teeth show that the early ooid layers grew on the Fe-oxide-impregnated parts of the teeth (Figs. 6, 7C, D). Actually, a similarity of shape and size exists between the observed rod-shaped phosphatic grains and some widespread genera of living Fe-reducing bacteria, like *Shewanella* and *Geobacter* (Chliders et al. 2002; Konhauser 2007). The main morphological difference between living taxa and the observed Cretaceous remains is the presence of a longitudinal groove in the latter. This feature could be a collapse feature due either to degradation of bacterial cells or to the shrinkage of a hydrated precursor phosphate phase that, during diagenesis, lost excess water. The microcracked appearance of phosphate supports the second hypothesis.

Collectively, these observations suggest that the microorganisms recorded as phosphate rods were Fe-reducing, organoheterotrophic bacteria that lived by coupling the oxidation of organic matter contained in the sediment with Fe-oxide reduction. These microbial communities started their metabolic activity in anoxic but not sulfidic (post-oxic) conditions, and promoted the reduction of Fe-oxide surfaces, which formed in a previous phase of oxidizing conditions. At the same time, the concentration of phosphate, delivered by bacterial decomposition of organic matter, increased in the pore waters. The release of additional phosphate ions, which are known to be adsorbed by Fe-oxides (Froelich et al. 1988; Föllmi 1996; Slomp et al. 1996), related to reduction of the latter, possibly led to a local supersaturation in phosphate. Phosphate

precipitation took place at the outer surfaces of the ooids and provided ideal conditions for the preservation of the microbial community. Low solubility of Ca-phosphate also enhanced its preservation during subsequent changes in environmental conditions, both more and less reducing than those promoting precipitation. In this sense, the preserved microbial community was not responsible for the growth of the ooids but, on the contrary, was related to a destructional stage as biocorrosion of Fe-rich layers. Precipitation of phosphate, partly enhanced by P delivered through Fe reduction, ended biocorrosion, chemically stabilized outer ooid surfaces, and thus contributed indirectly to their growth.

Alternating Fe-oxides and Ca-phosphate cortex portions would be the result of alternation of oxidizing (i.e., favorable to Fe-oxide precipitation) and post-oxic (triggering the proliferation of Fe-reducing bacteria and precipitation of phosphate) conditions. It seems unlikely that the thickest phosphate cortex portions (~ 250 μm) formed during a single phosphatization event. It is more likely that they record numerous additions of thin (~ 10 μm) Fe-oxide layers and their subsequent phosphatization. CL and BSE images show that even the most homogeneous phosphate portions are alternating phosphate and discontinuous Fe-oxide layers (Figs. 4B, 7).

These features allow speculation about processes of ooidal ironstone deposit formation (Fig. 12). These rocks are highly condensed deposits making part of a drowning sequence, 30-50 m thick, consisting mainly of glaucony-rich sediments and marking the transition from the Berriasian peritidal carbonate platform to the early Cenomanian slope limestone and marl couplets (Pasquini et al. 2004; Decarlis and Lualdi 2008). It developed in transgressive conditions in a sediment-starved open shelf a few tens of meters deep. Here, quiet pelagic or hemipelagic sedimentation was periodically punctuated by storm events that affected bottom sediments, resulting in effective winnowing and reworking and leaving a lag deposit consisting mainly of larger biogenic remains, such as fish teeth. While exposed at the oxygenated sea floor, they were coated with and impregnated by Fe-oxides and encrusted by benthic foraminifera (steps 1 and 2 in Fig. 12). Iron likely was delivered from emergent lands (Massif Central) located

to the northwest of the study area (Dardeau 1984). During subsequent low-energy episodes, fine-grained organic-rich sediment accumulated and Fe-oxide-rich grains were buried. In subbottom sediments organic matter was degraded and porewaters enriched in P. The development of post-oxic conditions just below the seafloor led to utilization of Fe-oxide grain surfaces by Fe-reducing bacteria (step 3a in Fig. 12). This process caused a release of P previously adsorbed on Fe-oxides, and hence a further local increase of phosphate concentration, which triggered phosphate precipitation on outer ooid surfaces (step 3b in Fig. 12).

The association in the same bed of ooids with very different composition and development of phosphate-rich versus Fe-rich portions provides the best evidence of a complex sedimentary history of prolonged reworking of sediments with mixing of ooids characterized by independent growth paths and attributed to chronologically distinct ooid formation stages (step 4 in Fig. 12), according to widely accepted genetic models (e.g., Gehring 1985; Donaldson et al. 1999; Collin et al. 2005). Winnowing and reworking are also obviously confirmed by the common presence of broken ooids and ooids with a nucleus consisting of fragments of other ooids.

The origin of phosphate in mixed ooids is a widely debated topic. Some authors consider the precipitation of phosphate as a postdepositional replacement diagenetic process (Champetier et al. 1987; Sturesson and Bauert 1994; Sturesson et al. 2000). Others suggest a primary and probably biogenic origin of phosphatic layers of mixed ooids (e.g., Burkhalter 1995). Here, the data support the latter hypothesis and argue for the importance of microbially induced phosphate precipitation due to the activity of heterotrophic Fe-reducing bacteria that resulted in release of P from both degraded organic matter and reduced Fe-oxides.

CONCLUSIONS

1) Mixed Fe-oxide-phosphate ooids from the Lower Cretaceous oolitic ironstones of the French Maritime Alps are macroscopically and microscopically indistinguishable from pure Fe-

oxide ooids. *In situ* quantitative chemical analyses (microprobe), mineralogical analyses (XRD and micro Raman spectroscopy), and other qualitative techniques (backscattered electron imaging, cathodoluminescence, epifluorescence) are required to define overall composition, relative proportions, and distribution of Fe-oxides and Ca-phosphate.

2) The nanofabric of Fe-oxide cortical layers, composed of platy crystals, is typical of inorganic hematite precipitation, whereas phosphate cortical layers, composed partly of micrometer-size, bacillus-like rods, suggest a biologically induced precipitation of Ca-phosphate. Fe-oxides, precipitated at the seafloor, were used by heterotrophic, Fe-reducing microbial colonies for their metabolism when sediments were buried below the seafloor. Porewaters were enriched in P through organic-matter decomposition and desorption from Fe-oxides, leading to Ca-phosphate precipitation.

3) These bacteria were not involved directly in the ooid growth but were driving a destructive, biocorrosional activity at the outer surface of the recently formed Fe-ooids. Phosphate precipitation stopped the biocorrosion process, contributed to the ooid growth, and exceptionally fossilized a thriving microbial community.

4) Fe-ooid-rich deposits are well known to be complex palimpsest sediments recording a prolonged reworking history. The exact identification of the possible mixed Fe-oxide-phosphate composition adds complexity to the existing genetic models. Mixed ooids record in fact a complex growth history during cyclic alternations of oxic and post-oxic geochemical conditions that are necessarily related to alternating sediment accumulation and ooid shallow burial, and winnowing phases with exposure at the seafloor. Their recognition is therefore instrumental in more complete and detailed paleoenvironmental-sedimentological interpretations of sedimentary successions containing oolitic ironstones.

ACKNOWLEDGMENTS

The authors thank Bosiljka Glumac, an anonymous reviewer, Editor Gene Rankey and Associate Editor Bruce Wilkinson for their constructive comments and suggestions that improved the manuscript. Linda Pastero and Piergiorgio Rossetti (Dipartimento di Scienze della Terra, Università di Torino), and Anna Fusconi (Dipartimento di Biologia Vegetale, Università di Torino) are kindly thanked for precious help in XRD, micro Raman spectroscopy, and epifluorescence microscopy respectively.

REFERENCES

Baturin, G.N., 1982, Phosphorites on the Seafloor: Origin, Composition, and Distribution: Amsterdam, Elsevier, 343 p.

Beyssac, O., Goffé, B., Chopin, C., and Rouzaud, J.N., 2002, Raman spectra of carbonaceous material in metasediments: a new geothermometer: Journal of Metamorphic Geology, v. 20, p. 859–871.

Bubenicek, L., 1971, Géologie du gisement de fer de Lorraine: Bulletin du Centre de Recherche de Pau, v. 5, p. 223–320.

Burkhalter, R.M., 1995, Ooidal ironstones and ferruginous microbialites: origin and relation to sequence stratigraphy (Aalenian and Bajocian, Swiss Jura mountains): Sedimentology, v. 42, p. 57-74.

Cayeux, L., 1936, Existence de nombreuses bactéries dans les phosphates sédimentaires de tout âge. Conséquences: Acadèmie des Sciences (Paris), Comptes Rendus, v. 203, p. 1198-1200.

Champetier, Y., Hamdadou, E., and Hamdadou, M., 1987, Examples of biogenic support of mineralization in two oolitic iron ores – Lorraine (France) and Gara Djebilet (Algeria): Sedimentary Geology, v. 51, p. 249-255.

Chliders, S.E., Clufo, S., and Lovley, D.R., 2002, *Geobacter metallireducens* accesses insoluble Fe(III) oxide by chemotaxis: Nature, v. 416, p. 767-769.

Collin, P.Y., Loreau, J.P., and Courville, P., 2005, Depositional environments and iron ooid formation in condensed sections (Callovian–Oxfordian, south-eastern Paris basin, France): Sedimentology, v. 52, p. 969-985.

Dahanayake, K., and Krumbein, W.E., 1985, Ultrastructure of a microbial mat-generated phosphorite: Mineralium Deposita, v. 20, p. 260-265.

Dahanayake, K., and Krumbein, W.E., 1986, Microbial structures in oolitic iron formations. Mineralium Deposita, v. 21, p. 85-94.

Dardeau, G., 1984, Alpes Maritimes, *in* Debrand-Passard, S., Courbouleix, S., and Lienhardt, M.J., eds., Synthèse Géologique du Sud-Est de la France: Bureau de Recherches Géologiques et Minières, Mémoires, v. 125, p. 1-255.

Dardeau, G., 1988, Tethyan evolution and Alpine reactivation of Jurassic extensional structures in the French “Alpes maritimes”: Société Géologique de France, Bulletin, v. 4, p. 651-657.

Debelmas, J., and Kerckhove, C., 1980, Les Alpes franco-italiennes, *in* France: Introduction à la Géologie du Sud-Est: Géologie Alpine, v. 56, p. 21-58.

Decarlis, A., and Lualdi, A., 2008, Stratigraphy and deposition of lower Cretaceous condensed deposits in the Maritime Alps (Nice arc, SE France): Società Geologica Italiana, Bollettino, v. 127, p. 13-24.

de Riaz, A., 1900, Nouvelles observations sur le système crétacé dans les Alpes-Maritimes: Société Géologique de France, Bulletin, v. 18, p. 764-765.

Donaldson, W.S., Plint, A.G., and Longstaffe, F.J., 1999, Tectonic and eustatic control on deposition and preservation of Upper Cretaceous ooidal ironstone and associated facies: Peace River Arch area, NW Alberta, Canada: Sedimentology, v. 46, p. 1159-1182.

Einsele, G., 2000, Sedimentary Basins; Evolution, Facies, and Sediment Budget, Second Edition: New York, Springer-Verlag, 792 p.

Föllmi, K.B., 1996, The phosphorus cycle, phosphogenesis and marine phosphate-rich deposits: Earth-Science Reviews, v. 40, p. 55-124.

Froelich, P.N., Arthur, M.A., Burnett, W.C., Deakin, M., Hensley, V., Jahnke, R., Kaul,. L., Kim, K.-H., Roe, K., Soutar, A., and Vathakanon, C., 1988, Early diagenesis of organic matter in Peru continental margin sediments: phosphorite precipitation: Marine Geology, v. 80, p. 309-343.

Fürsich, F., 1971, Hartgründe und Kondensation im Dogger von Calvados: Neues Jahrbuch für Geologie und Paläontologie, Abhandlüngen, v. 138, p. 313-342.

Gehring, A.U., 1985, A microchemical study of iron ooids: Eclogae Geologicae Helvetiae, v. 78, p. 451-457.

Horton, A., Ivimey-Cook, H.C., Harrison, R.K., and Young, B.R., 1980, Phosphatic öoids in the Upper Lias (Lower Jurassic) of central England: Geological Society of London, Journal, v. 137, p. 731-740.

Karakus, M., Hagni, R.D., and Spreng, A.C., 2001, Cathodoluminescence petrography and chemistry of the phosphate grains in the Lower Jurassic (Aalenian) ironstones of Lorraine, France, *in* Hagni, R.D., ed., Studies on Ore Deposits, Mineral Economics, and Applied Mineralogy: with Emphasis on Mississippi Valley-Type Base Metal and Carbonatite-Related Ore Deposits: University of Missouri-Rolla, p. 335-363.

Konhauser, K., 2007, Introduction to Geomicrobiology: Oxford, U.K., Blackwell Publishing, 425 p.

Krajewski, K.P., Van Cappellen, P., Trichet, J., Kuhn, O., Lucas, J., Martín-Algarra, A., Prévôt, L., Tewari, V.C., Gaspar, L., Knight, R.I., and Lamboy, M., 1994, Biological processes and apatite formation in sedimentary environments: Eclogae Geologicae Helvetiae, v. 87, p. 701-745.

Lanteaume, M., 1968, Contribution à l'étude géologique des Alpes Maritimes franco-italiennes: Service de la Carte Géologique de France, Paris, Mémoires, 405 p.

Lucas, J., and Prévôt, L.E., 1985, The synthesis of apatite by bacterial activity: mechanism: Sciences Géologiques: Mémoires, v. 77, p. 83-92.

Lucas, J., and Prévôt, L.E., 1991, Phosphates and fossil preservation, *in* Allison, P.A., and Briggs, D. E. G., eds., Taphonomy: Releasing the Data Locked in the Fossil Record: New York, Plenum Press, p. 389-409.

Pasquini, C., Lualdi, A., and Vercesi, P.L., 2004, Depositional dynamics of glaucony-rich deposits in the Lower Cretaceous of the Nice arc, southeast France: Cretaceous Research, v. 25, p. 179- 189.

Perez, A., 1847, Atti della ottava riunione degli scienziati italiani. Tipografia Ferrando, Genova, p. 651-658.

Préat, A., Mamet, B., De Ridder, C., Boulvain, F., and Gillan, D., 2000, Iron bacterial and fungal mats, Bajocian stratotype (Mid-Jurassic, northern Normandy, France): Sedimentary Geology, v. 137, p. 107-126.

Purnachandra Rao, V., Naqvi, S.W.A., Dileep Kumar, M., Cardinal, D., Michard, A., Borole, D.V., Jacobs, E., and Natarajan, R., 2000, A comparative study of Pleistocene phosphorites from the continental slope off western India: Sedimentology, v. 47, p. 945-960.

Schulz, H.N., and Schulz, H.D., 2005, Large sulfur bacteria and the formation of phosphorite: Science, v. 307, p. 416-418.

Slomp, C.P., Epping, E.H.G., Helder, W., and Van Raaphorst, W., 1996, A key role for iron-bound phosphorus in authigenic apatite formation in North Atlantic continental platform sediments: Journal of Marine Research, v. 54, p. 1179-1205.

Soudry, D., 1992, Primary bedded phosphorites in the Campanian Mishash Formation, Negev, southern Israel: Sedimentary Geology, v. 80, p. 77-88.

Soudry, D., 2000, Microbial Phosphate Sediments, *in* Riding, R.E., and Awramik, S.M., eds., Microbial Sediments: Berlin, Springer-Verlag, p. 127-136.

Soudry, D., and Champetier, Y., 1983, Microbial processes in the Negev phosphorites (southern Israel): Sedimentology, v. 30, p. 411-423.

Sturesson, U., and Bauert, H., 1994, Origin and palaeogeographical distribution of the Viruan iron and phosphate ooids in Estonia: evidence from mineralogical and chemical compositions: Sedimentary Geology, v. 93, p. 51-72.

Sturesson, U., Dronov, A., and Saadre, T., 1999, Lower Ordovician iron ooids and associated oolitic clays in Russia and Estonia: a clue to the origin of iron oolites?: Sedimentary Geology, v. 123, p. 63-80.

Sturesson, U., Heikoop, J.M., and Risk, M.J., 2000, Modern and Palaeozoic iron ooids – a similar volcanic origin: Sedimentary Geology, v. 136, p. 137-146.

Teyssen, T.A.L., 1984, Sedimentology of the Minette oolitic ironstones of Luxembourg and Lorraine: a Jurassic subtidal sandwave complex: Sedimentology, v. 31, p. 195-211.

Thomel, G., 1961, *Lyticoceras corroy* nov. sp. de l'Hauterivien niçois: Société Géologique de France, Bulletin, v. 3, p. 468-473.

Van Houten, F.B., 1990, Palaeozoic oolitic ironstones on the North American Craton: Palaeogeography, Palaeoclimatology, Palaeoecology, v. 80, p. 245–254.

Van Houten, F.B., and Bhattacharyya, D.P., 1982, Phanerozoic oolitic ironstones - Geologic record and facies model: Annual Review of Earth and Planetary Sciences, v. 10, p. 441-457.

CAPTIONS OF FIGURES

Fig. 1.–Geographic and geological setting. **A)** Location of the study area (squared and arrowed) in the context of the Western Alps main units. **B)** Geographical location of the studied sections in the study area (AL, Albaretta; RN, Roccaniera) and of the classic section of Saint Laurent de l'Escarène (SL).

Fig. 2.–Stratigraphic succession in the study area and detail of the Lower Cretaceous condensed interval.

Fig. 3.–Weathered outcropping bedding surface of the Lower Cretaceous deposits showing the oblate ellipsoidal Fe-ooids. Note also the burrows (arrowed), corresponding to ooid-poor portions, and a reworked internal ammonite mold.

Fig. 4. –Cross section through an ooid showing a structureless angular clast of Fe-oxyhydroxides at its nucleus and the characteristic laminar cortex. Note: concavo-convex contacts (arrows) between the largest ooid and the smaller ones at the top left and bottom right with evidence of plastic deformation; the asymmetric development of discrete sets of cortical layers that cannot be followed all around the larger ooid; in the inset, a sketch of the latter shows the successive stages of growth through which an equidimensional nucleus gave rise to a markedly oblate ellipsoidal ooid. **A)** Photomicrograph in convergent transmitted light (CTL) that minimizes the light absorption by Fe-oxides and allows to better distinguish the ooid internal structure. Darker layers generally correspond to greater abundance of Fe-oxides. **B)** Backscattered electron (BSE) image highlighting the abundance of Fe in the nucleus and in the outer cortical portion (brighter), and the phosphate-rich middle cortical portion (darker). At a smaller scale, an alternation, albeit irregular, of brighter and darker layers can be noted.

Fig. 5.–CTL photomicrograph of Fe-ooid cortex with an encrusting foraminifer replaced by Fe-oxides (indicated by arrow).

Fig. 6.–BSE image of a Fe-ooid with a fish tooth in the nucleus. Note: the dark color of the phosphatic, enamel part; the tubular aspect of the dentine part, impregnated by bright Fe-oxides; the preferential growth of the early layers of the ooids on the Fe-oxide-impregnated side of the tooth; the alternation of Fe-rich (brighter) and phosphate-rich (darker) concentric cortical layers.

Fig. 7.– Comparison of mixed Fe-oxides-phosphate ooids imaged by different techniques (CTL, CL, BSE, epifluorescence) aimed to better illustrate distribution of Fe-oxides and Ca-phosphate. **A-D)** Mixed Fe-oxide-phosphate ooids, some with a fish tooth in the nucleus, as seen in CTL **(A)**, CL **(B)**, BSE **(C)**, and epifluorescence using a B-2A filter **(D)**. Note the moderate blue cathodoluminescence and darker BSE color of the tooth and phosphate layers in contrast to nonluminescence and brighter BSE color of Fe-oxides as well as the fluorescence of the phosphate, both biogenic (tooth) and diagenetic (ooid cortical layers) compared to nonfluorescence of Fe-oxides. **E, F)** BSE **(E)** and CL **(F)** images of a mixed Fe-oxide-phosphate ooid. Note the good correspondence of blue cathodoluminescence and darker BSE colors of phosphate portions. **G, I)** CL image of mixed Fe-oxide-phosphate ooid showing the very different composition of adjacent ooids due to the diverse development of phosphate-rich versus Fe-rich portions. The white arrow points to the lateral discontinuity of a Fe-oxide cortical layer that transitions into phosphate. **H, J)** Black and white epifluorescence images, taken using a G-2A filter, of the squared areas in Parts G and I respectively. Note the bright fluorescence of the blue-cathodoluminescing phosphate-rich portions.

Fig. 8.–Raman spectrum of poorly crystalline carbonaceous material, as shown by the intense and broad bands occurring at around 1350 cm^{-1} (D1 band) and near 1600 cm^{-1} (G band) (cf. Beyssac et al. 2002, with references). The narrow peak at 964 cm^{-1} is instead related to apatite.

Fig. 9.–SEM image of a Fe-oxide-rich ooid layer. Note the platy habit of hematite crystals.

Fig. 10.–SEM images of broken unetched surfaces of mixed Fe-oxide-phosphate ooids. **A)** Cross section, about 30 µm thick, through a mixed ooid that highlights the alternation of Fe-rich layers characterized by the platy crystal habit, and phosphate-rich layers with smoother, microcracked surfaces (arrow). **B)** Closeup of the square area from **(A)** that shows the association of platy Fe-oxides and the microcracked phosphates. Note that Fe-oxide plates are coated by a thin film of phosphate. **C)** Outer surface of a phosphate-rich cortical layer composed of micrometer-size, rod-shaped particles. **D, E, F)** Outer surface of a phosphate-rich cortical layer showing clustering of rods, random in Parts D and E or forming chains (Part F) (arrow). **G, H)** Closeup of phosphate rods with common curved shape and a central groove. Note the microcracking of the entire phosphate layer surface. **I)** Bowl- and filament-shaped phosphate particles in a phosphate-rich layer.

Fig. 11.–High magnification CTL photomicrograph showing the alternation of pure Fe-oxide layers (white arrows), a few micrometers thick and laminated, with mixed phosphate- Fe-oxide layers characterized by a spongy structure (black arrows). Microcavities are filled with phosphate and suggest a process of “corrosion” of Fe-oxide layers.

Fig. 12.– Conceptual model of formation of mixed Fe-oxide-phosphate ooids. Upper panel shows processes taking place on the seafloor and just below it. Lower panel shows microscale

diagenetic and microbiological processes. Figures 3a and 3b depict biocorrosion of Fe-oxide by Fe-reducing bacteria, followed by phosphate precipitation.

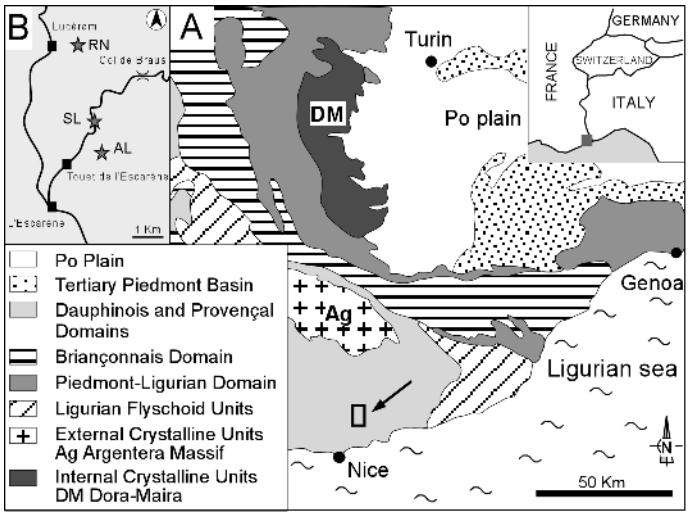
B
A
RN
SL
AL
1 Km
DM
Turin
Po plain
FRANCE
GERMANY
SWITZERLAND
ITALY
Genoa
Ag
Ligurian sea
Nice
50 Km
Po Plain
Tertiary Piedmont Basin
Dauphinois and Provençal Domains
Briançonnais Domain
Piedmont-Ligurian Domain
Ligurian Flyschoid Units
External Crystalline Units
Ag Argentera Massif
Internal Crystalline Units
DM Dora-Maira

Fig. 1

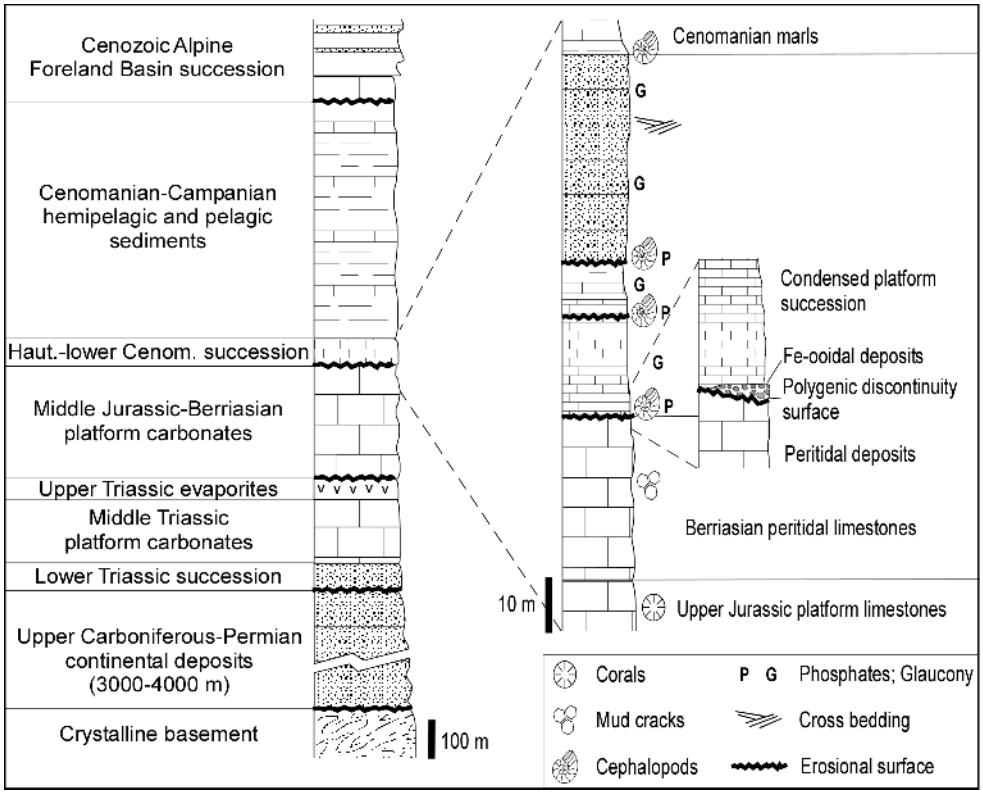
Cenozoic Alpine
Foreland Basin succession
Cenomanian-Campanian
hemipelagic and pelagic
sediments
Haut.-lower Cenom. succession
Middle Jurassic-Berriasian
platform carbonates
Upper Triassic evaporites
Middle Triassic
platform carbonates
Lower Triassic succession
Upper Carboniferous-Permian
continental deposits
(3000-4000 m)
Crystalline basement
100 m
10 m
Cenomanian marls
G
G
P
G
P
G
P
Condensed platform
succession
Fe-ooidal deposits
Polygenic discontinuity
surface
Peritidal deposits
Berriasian peritidal limestones
Upper Jurassic platform limestones
Corals
Mud cracks
Cephalopods
P G
Phosphates; Glaucony
Cross bedding
Erosional surface

Fig. 2

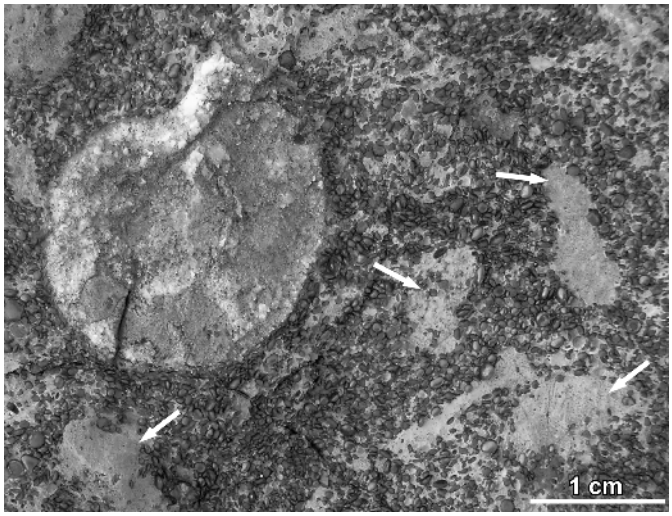

Fig. 3

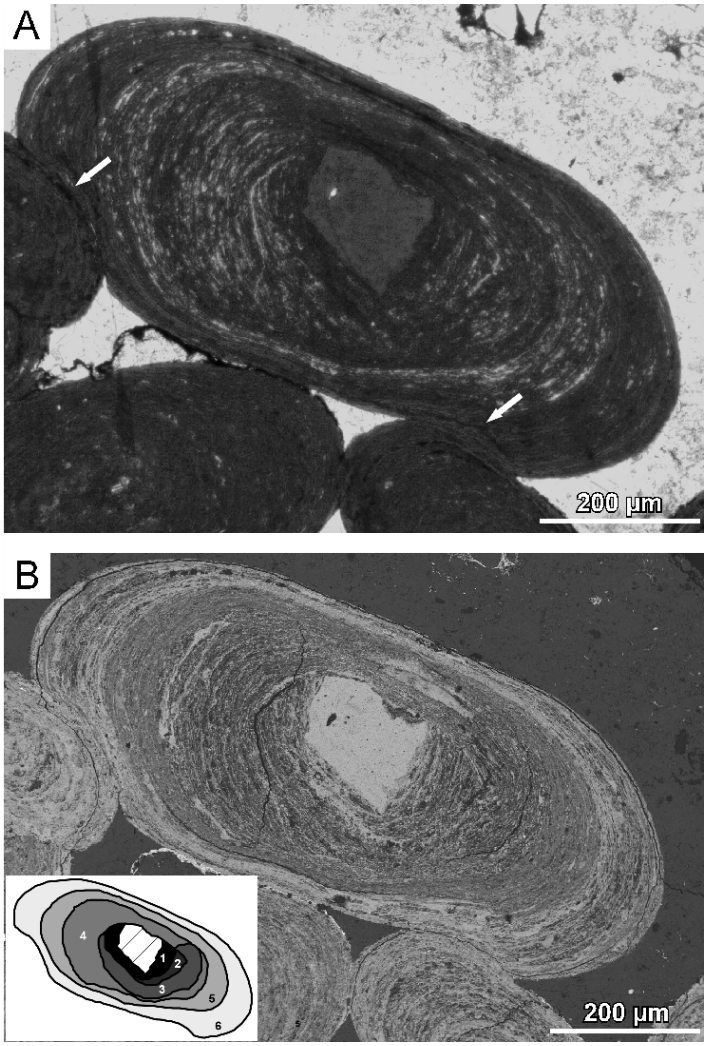

Fig. 4

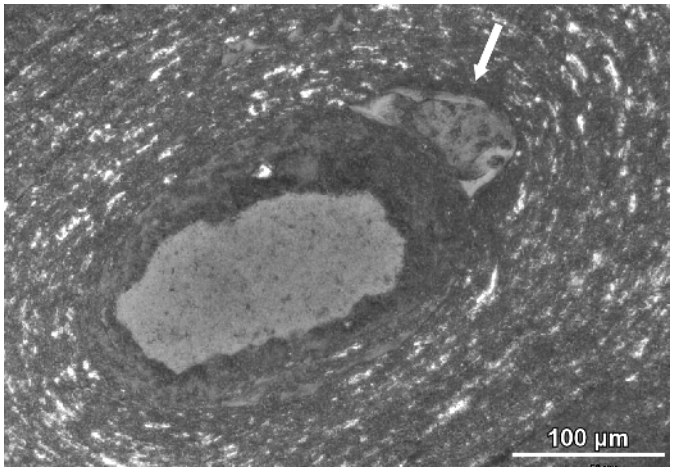

Fig. 5

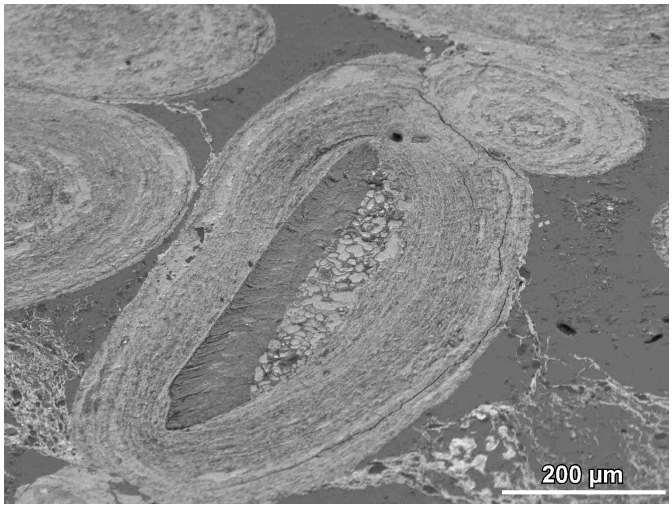

Fig. 6

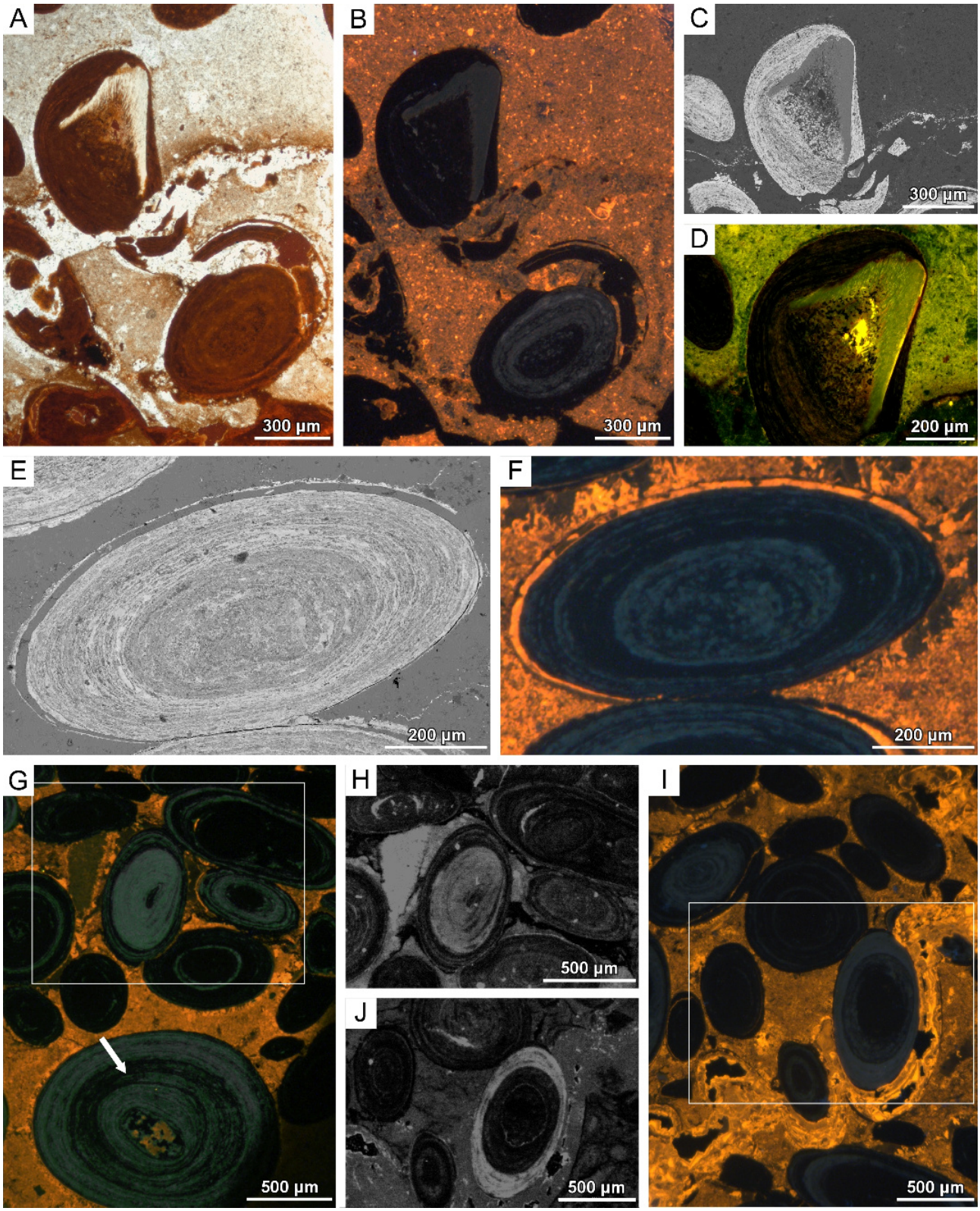
A
300 µm
B
300 µm
C
300 µm
D
200 µm
E
200 µm
F
200 µm
G
500 µm
H
500 µm
J
500 µm
I
500 µm

Fig. 7

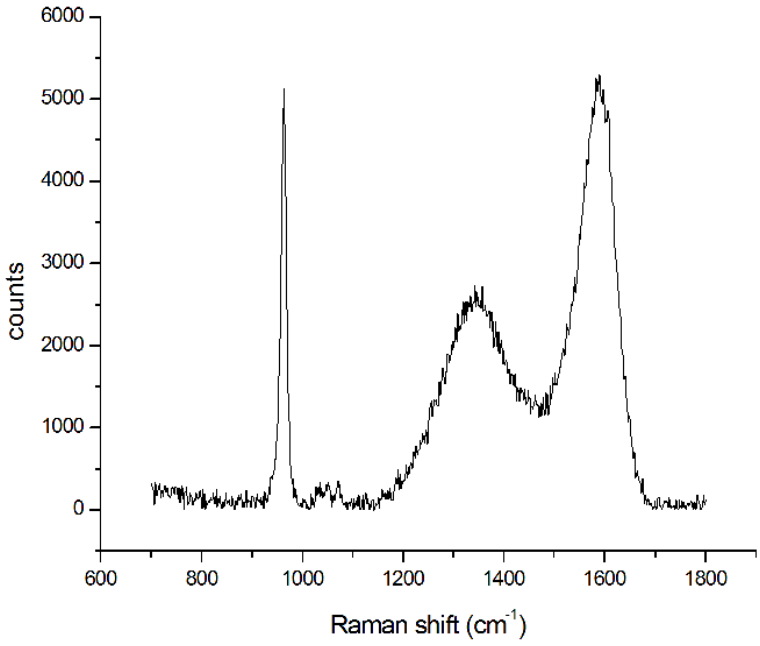
6000
5000
4000
3000
2000
1000
0
counts
600
800
1000
1200
1400
1600
1800
Raman shift (cm-1)

Fig. 8

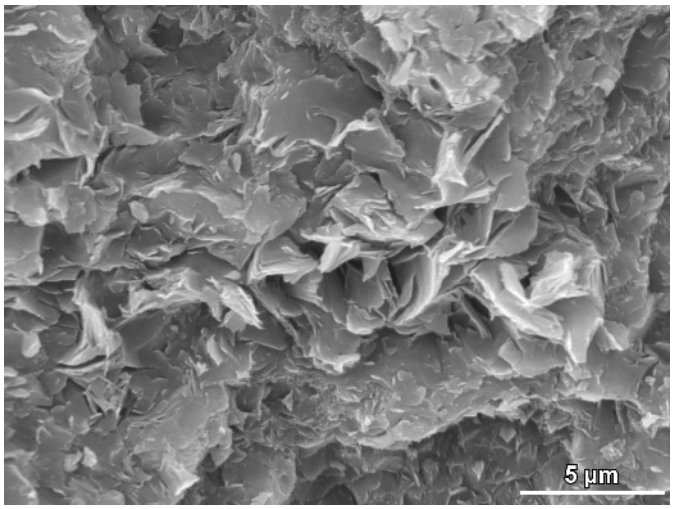

Fig. 9

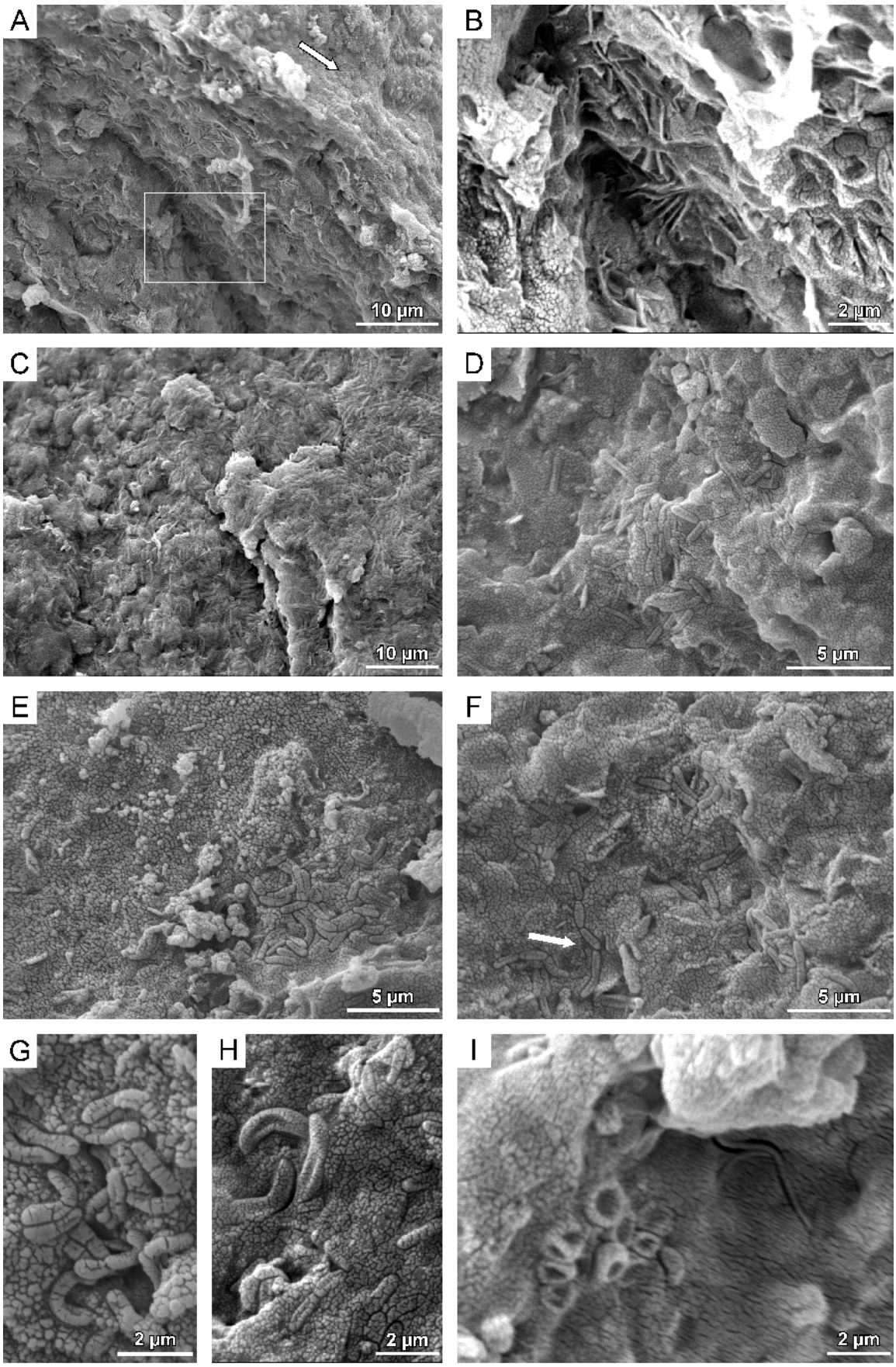

Fig. 10

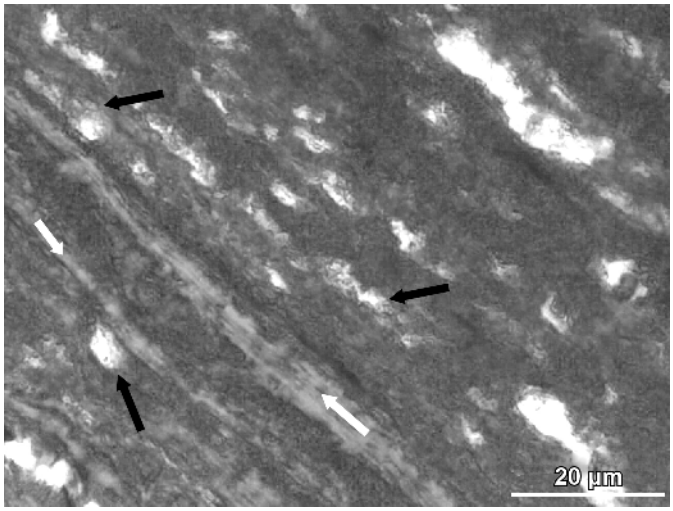

Fig. 11

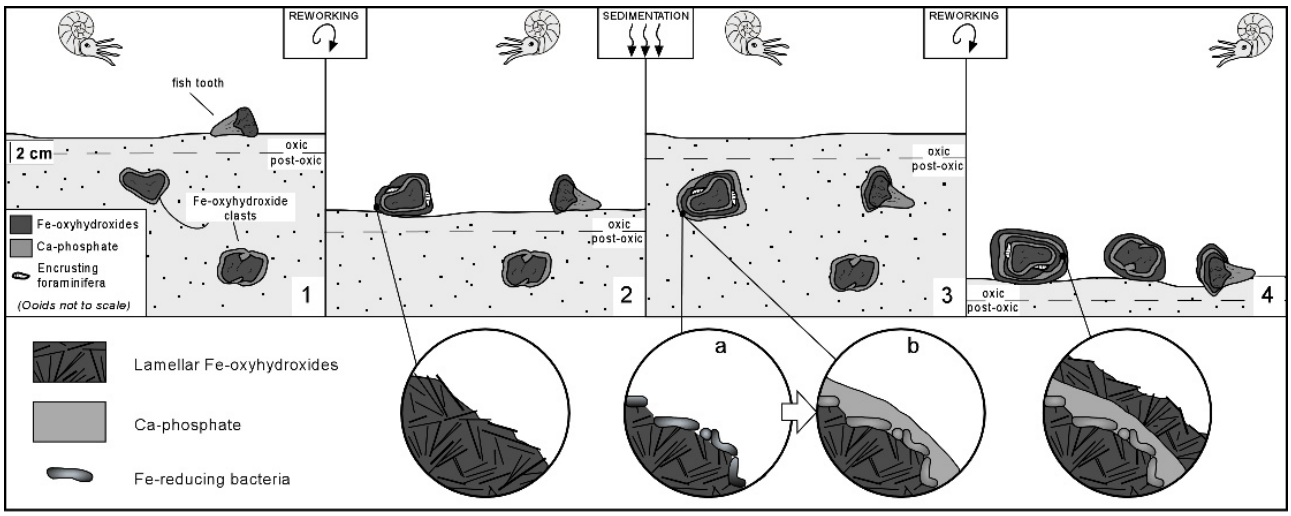
REWORKING
SEDIMENTATION
REWORKING
fish tooth
2 cm
oxic
post-oxic
Fe-oxyhydroxide clasts
Fe-oxyhydroxides
Ca-phosphate
Encrusting foraminifera
(Ooids not to scale)
1
2
3
4
a
b
Lamellar Fe-oxyhydroxides
Ca-phosphate
Fe-reducing bacteria

Fig. 12